Exciplex Stabilization in Asymmetric Acene Dimers

Rachel Ann Krueger, and Guillaume Blanquart

Just Accepted

Exciplex Stabilization in Asymmetric Acene Dimers

Rachel A. Krueger[†] and Guillaume Blanquart[*,‡]

Department of Chemistry, California Institute of Technology, Pasadena, California 91125, United States, and Department of Mechanical Engineering, California Institute of Technology, Pasadena, California 91125, United States. Phone: 1-626-395-4306. Email: g.blanquart@caltech.edu

Abstract

Excimers play an important role in photochemical processes ranging from singlet fission to DNA damage, and the characteristic red shift in fluorescence spectra associated with excimer formation can provide information about aggregate formation and the orientation of chromophores. When a mixture of chromophores is present, exciplex formation may lead to spectral characteristics distinct from those of either monomer or the corresponding excimers. To predict the effects of aggregation in a system containing a mixture of small acenes, binding energies and minimum-energy geometries have been calculated for three mixed S_1 exciplexes. Benchmark CASSCF/NEVPT2 multireference binding energies of 18.2 kJ/mol, 27.7 kJ/mol, and 49.3 kJ/mol are reported for the benzene-naphthalene, benzene-anthracene, and naphthalene-anthracene exciplexes, respectively. TDDFT calculations have been performed using a range of exchange-correlation functionals, showing that many functionals perform inconsistently, and the error in binding energy often depends on the character of the monomer excitation from which the exciplex

---

[*]To whom correspondence should be addressed

[†]Department of Chemistry, California Institute of Technology, Pasadena, California 91125, United States

[‡]Department of Mechanical Engineering, California Institute of Technology, Pasadena, California 91125, United States. Phone: 1-626-395-4306. Email: g.blanquart@caltech.edu

state is derived. Moderate exciplex stabilization observed for the benzene-naphthalene and naphthalene-anthracene exciplexes results from a mixture of charge transfer and exciton delocalization.

1. Introduction

Characterization of exciplexes represents an important step in understanding the dynamic photophysical and photochemical processes of multi-chromophore systems. Exciplex formation occurs when two or more molecules are involved in a photoabsorption event, often but not necessarily beginning when the absorption of one molecule perturbs the electronic state of a neighbor. The resulting structure is called an excimer—an excited dimer—in the case that the molecules involved are identical, or as an exciplex—an excited complex—in other cases. The wave function for an arbitrary exciplex containing molecules P and Q may be described as a combination of Frenkel excitations, in which electrons are excited from donor orbitals into acceptor orbitals located on the same molecule, P^*Q and PQ^*, and charge transfer states, in which the donor and acceptor orbitals lie on different molecules, $P^{\cdot-}Q^{\cdot+}$ and $P^{\cdot+}Q^{\cdot-}$.[1,2] Exciplex formation often results in the stabilization of complexes at geometries that would be unfavorable or repulsive in the ground state.[1,3]

Recent interest in exciplex formation has been driven by efforts to determine singlet fis-

sion mechanisms, in which exciplexes represent intermediate or trap states in the conversion of a singlet exciton into two lower-energy triplet excitons.[4–7] Long-lived charge-transfer-dominated exciplexes have been observed in photoexcited DNA and RNA strands.[8]

In laser-induced fluorescence (LIF) experiments, excimer emission produces broad, structureless peaks that are red-shifted with respect to the corresponding emissions from the parent molecules due to excimer stabilization.[9] In experiments involving a single chromophore, excimer fluorescence is readily identified. When a wide range of chromophores are present, complexes containing two different chromophores are likely to be more prevalent than dimers of a single chromophore,[10] and it it not *a priori* apparent whether the emission from these complexes will be distinguishable from the parent monomer emissions. This question is of paramount importance for combustion systems, where LIF represents a promising technique for characterizing soot precursors,[11] which might consist of PAH van der Waals dimers[12] or even pairs of PAHs connected by aliphatic linkers[13] capable of forming intramolecular exciplexes.

Accurately assigning fluorescence peaks, though, will require a broad database of exciplex binding energies, the major contributor to the characteristic redshift.[9,10] Exciplex binding energy is defined here as the potential energy difference between the minimum energy exciplex configuration and the two separated monomers, one of them excited.

For ground state complexes, a roughly linear scaling relationship between PAH molecular weight and noncovalent dimer binding energy has emerged for several homodimers,[14,15] the benzene-naphthalene heterodimer,[16] and the naphthalene-anthracene heterodimer.[17] For PAH exciplexes, though, the effects of monomer substitution remain unclear—no binding energies have yet been reported for mixed exciplexes containing small, unsubstituted PAHs.

Because of the large number of exciplexes that may be formed from even a moderate number of small PAHs, characterizing each one experimentally would represent a monumental task. Obtaining accurate theoretical estimates of im-

portant exciplexes represents a way forward, provided that computationally tractable methods with acceptable accuracy are available.

To date, most *ab initio* studies have focused on the smallest acene excimers. Binding energies and singlet excitation energies for the benzene S_1 excimer have been characterized using CASPT2,[18,19] coupled cluster methods,[20] and equation-of-motion coupled cluster methods.[21] Binding energies have been evaluated at the global minimum potential energy configuration for the excimer, corresponding to an eclipsed configuration, with one monomer translated along the intermolecular coordinate with respect to the other. The results range from 33-48 kJ/mol[19,20] when corrected for basis set superposition error (BSSE) by the counterpoise (CP) method.[22] Even the lowest binding energy obtained is more than twice as large as the CP-corrected benchmark CCSD(T) binding energies obtained for the ground state benzene dimer in a parallel-displaced configuration.[23]

Naphthalene and larger acenes are characterized by two close-together, low-lying singlet $\pi \rightarrow \pi^*$ excited states, polarized along the two axes of the molecules. The B_{2u} state, labeled L_a, is described almost completely by a HOMO→LUMO transition, while the B_{3u} L_b state is the result of a mixed HOMO-1→LUMO and HOMO→LUMO+1 transition. In the valence-bond theory framework, the L_a state is ionic and the L_b state covalent.[24]

Time-dependent density functional theory (TDDFT) calculations performed using hybrid exchange-correlation functionals tend to underestimate the energy of the L_a state, and this error increases with increasing acene size.[25,26] Although the ionic description of the state hints at charge separation, the L_a state cannot be classified as a "true" charge transfer state,[27,28] indicating that the error is not directly attributable to the well-known failure of hybrid TDDFT to capture charge transfer behavior. Use of double-hybrid functionals improves L_a energies substantially.[25,29]

The energy of the L_b state, on the other hand, tends to be overestimated by TDDFT calculations using hybrid, double-hybrid, and range-separated functionals. Errors remain roughly

constant with acene size. For several hybrid functionals, the combination of errors in both state energies leads to the incorrect L_a–L_b state ordering for the naphthalene monomer.[25,26]

For the naphthalene excimer $(NN)^*$, the L_a and L_b-derived states cross at an intermolecular separation of 4.5 Å,[30,31] and the L_a-derived state becomes the lowest-energy singlet excited state around the potential energy minimum at an intermolecular separation of $\approx$ 3.08 Å. CASPT2 calculations yielded non-CP-corrected binding energies of 128 kJ/mol and 60 kJ/mol for the L_a and L_b-derived states of the naphthalene excimer, respectively.[30]

The lowest singlet excited state of the benzene-naphthalene exciplex is derived from the L_b state of the naphthalene monomer. An approximate CP-corrected NEVPT2 complete basis set binding energy of 19.2 kJ/mol has been reported for the complex in the S_1 state,[32] indicating a much weaker interaction than the ones observed for S_1 benzene and naphthalene excimers.

The first objective of this work is to evaluate the effectiveness of TDDFT for calculating exciplex binding and excitation energies using several exchange-correlation functionals. Three representative acene exciplexes have been selected for study: the benzene-naphthalene exciplex $(BN)^*$, the benzene-anthracene exciplex $(BA)^*$, and the naphthalene-anthracene complex $(NA)^*$. TDDFT binding energies are compared against CASSCF/NEVPT2 results. Binding energies have also been calculated using the second-order algebraic diagrammatic construction method, $(ADC(2))$,[33] a complementary single-reference approach. To the best of our knowledge, these binding energies are the first to be reported for $(BA)^*$ and $(NA)^*$.

To rationalize trends in exciplex binding energies, the extent of the exciton delocalization and charge transfer in each complex has been quantified using the one-electron transition density matrix. Developing a predictive model for spectroscopic parameters of arbitrary aromatic exciplexes will require a larger body of data, but the benchmark results and systems characterized in this work represent a first step towards this goal.

2. Computational Methods

To avoid the pitfalls associated with the lowest-energy electronic states of the small acenes, multireference complete active space self-consistent field (CASSCF) calculations with a perturbative n-electron valence perturbation theory second-order (NEVPT2) correction[34] have been performed to provide a reliable point of comparison for TDDFT results. Benchmarks have shown that the NEVPT2 method yields perturbative dynamic correlation values similar to the popular CASPT2 method,[35] but the Dyall Hamiltonian used in NEVPT2 prevents intruder state mixing and eliminates the need for shift parameters.[34] Perturbatively-corrected CASSCF calculations have the capacity to capture both static and dynamic correlation, providing a balanced treatment of both the single and double excitations observed among acenes. Standard EOM-CCSD potential energy curves flip the order of the lowest-energy singlet excited states of the naphthalene excimer around the global minimum geometry, an error that CASSCF/CASPT2 calculations correct.[30] For the relative energy of the lowest-energy singlet excited state of benzene, EOM-EE-CCSD and NEVPT2 calculations vary by less than 2 kJ/mol.[21,35] All CASSCF wave functions were further optimized in CASCI calculations to adjust orbital coefficients before NEVPT2 corrections were calculated.

The CASSCF/CASCI/NEVPT2 techniques used here have been employed in previous work,[32] and only a brief review will be provided. This multireference procedure is used here in order to calculate complete binding curves for $(BN)^*$, $(BA)^*$, and $(NA)^*$ using the cc-pVDZ basis set,[36] data that is reported here for the first time. The use of a relatively small basis set to describe noncovalent interactions might rightly provoke skepticism. However, it has been shown that, for aromatic exciplexes, cancellation of BSSE and basis set incompleteness error yields cc-pVDZ binding energies very close to the complete basis set limit, providing an excellent cost–accuracy trade-off.[32] Energies calculated according to this procedure will be described simply as NEVPT2 energies.

The active spaces for multireference calculations include one p orbital parallel to the intermolecular axis and one electron for each carbon atom. Smaller active spaces yield the wrong state ordering for naphthalene complexes.[30] The resulting active spaces range in size from 16 active orbitals and electrons to 24 active orbitals and electrons.

To make these large active spaces computationally tractable, the density matrix renormalization group (DMRG) approach[37–39] was used in both CASSCF and NEVPT2 calculations. By employing an approximate wave function ansatz known as the matrix product state (MPS), the DMRG method offers a polynomial-scaling alternative to exponentially-scaling CAS methods. The accuracy of the wave function is determined by the dimension chosen for the matrices, known as the bond dimension M. For a discussion of the errors associated with the DMRG approach and the convergence of DMRG results with increasing M, the reader is referred to recent discussions of the method.[40,41] The number of variational parameters scales as M^2. An approximate compressed MPS perturber[40] was used in NEVPT2 calculations, which were of the strongly contracted type. DMRG calculations were performed using the Pyscf framework version 1.3b[42] with an interface to the Block DMRG solver version 1.5.0.[43]

CASSCF starting orbitals were obtained from restricted Hartree Fock (RHF) calculations, and active space p orbitals were selected using the atomic valence active space (AVAS) technique.[44] The choice of starting orbital type can affect the convergence of DMRG energies with increasing M, but aromatic exciplex binding energies computed using canonical and localized starting orbitals are both generally well-converged with $M = 500$ for CASSCF calculations and $M = 1200$ for CASCI and NEVPT2 calculations.[32] For the larger (NA)* exciplex, setting $M = 1000$ for the CASSCF step was necessary to obtain a converged binding energy, and localized B3LYP starting orbitals were used because RHF orbitals generated were of poor quality. For (BA)*, the binding energy calculated using both sets of conditions differed by

less than 1 kJ/mol, so the full binding curve was generated using $M = 500$ for the CASSCF step and RHF starting orbitals.

For TDDFT calculations, representative functionals from several major classes have been chosen. The B3LYP functional[45] has been chosen from the hybrid GGAs, as well as the BHandHLYP functional, with includes a larger amount of Hartree-Fock exchange than other hybrids.[46] The B2PLYP functional[47] with a double excitation correction[48] was chosen from the double hybrids. Grimme's D3 empirical dispersion correction with Becke-Johnson damping[49] was applied to the B3LYP, B2PLYP, and BHandHLYP functional results. Though developed for ground state DFT calculations, the D3 correction has also significantly improved the TDDFT description of excimers, at least for dimers in valence excited states such as the ones considered in this work.[50,51] To accelerate double hybrid calculations, the resolution of identity (RI) approximation[52] was used in the evaluation of Coulomb integrals.

Range-separated functionals have shown particular promise for describing the electronic states of aromatic systems.[27] Among these functionals, the ωB97 functional,[53] which includes varying Hartree-Fock exchange for all long-range interactions, and the ωB97X-D3 functional,[54] which includes a region of fixed Hartree-Fock exchange, were used.

To control the transition between long-range exact exchange and short-range semilocal exchange, range separated functionals rely on the use of a range-split parameter γ. Tuning γ values for individual systems to enforce as closely as possible the DFT version of Koopmans' theorem has been shown to improve the accuracy of range-separated functionals.[27,55]

To examine the effectiveness of this technique for exciplex binding energy calculations, the long-range corrected BLYP functional, LC-BLYP,[56] has been used, along with two variants of the LC-BLYP functional, each with γ tuned to minimize the difference between the energy of the highest-occupied molecular orbital in the ground state and the ground state ionization energy. For one of the functionals, LC-BLYP-TM, the tuning is performed only for the larger

monomer in each complex. For the other, LC-BLYP-TD, tuning is performed for the complete dimer at its minimum-energy geometry. Values of γ used in each functional for each exciplex are reported in Table S1. Optimal γ values do depend on the intermolecular separation of the complex, with γ for the dimer approaching γ for the larger monomer at an intermolecular separation of 10 Å. To prioritize correct treatment of the exciplexes near their energy minima, we have chosen to set γ for the LC-BLYP-TD functional to the optimal value obtained for the minimum-energy dimer configuration.

The def2-TZVP[57] basis set has been used for all TDDFT calculations, with the def2/JK auxiliary basis[58] used in RI calculations. TDDFT energies are generally less sensitive to basis set size than wave function methods. For electronic transition energies in a range of organic molecules, the def2-TZVP basis generally yields small errors with respect to the much larger aug-cc-pVTZ basis, providing excellent accuracy relative to computational cost.[59] Based on a benchmark study involving the ground state binding energies of the S66 noncovalent dimer test set, BSSE is expected to represent $\leq 12\%$ of the total binding energy.[60] The Tamm-Dancoff approximation was applied in all TDDFT calculations.

As an alternative single-reference approach, the ADC(2) method[33] was used together with the smaller cc-pVDZ basis set[36] because of the method's high memory requirements.[25,33] ADC(2) excitation energies were added to MP2 ground state energies, which are consistent with the ADC(2) reference state.[61]

All TDDFT and ADC(2) calculations were performed using the ORCA software package[62] version 4.0.0 with integration grid size 5. Statistical descriptors of exciton character were calculated using the TheoDORE package version 1.0.[63] Molecule graphics have been generated using VMD version 1.9.1.[64]

Previous studies of aromatic excimers have shown that an eclipsed configuration is the most favorable geometry for complexes in the lowest singlet excited state,[65–68] while parallel-displaced configurations have larger binding energies in the ground state for most acenes.[14,66] Exciplex geometries considered in this work (Fig. 1) resemble the minimum-energy structures for acene excimers, although the monomer size mismatch in the exciplex structures means that the larger monomer is not perfectly eclipsed by the smaller one. For $(BA)^*$, two eclipsed configurations are possible. The configuration with the benzene centered over the middle ring of the anthracene was chosen because its binding energy is greater than the binding energies of configurations with the benzene centered over a side ring.

Binding curves were generated by translating the monomers along the intermolecular coordinate r_z, with intramolecular coordinates frozen at their ground state values. Ground state monomer geometries were computed with DFT using the B3LYP functional and the def2-TZVP basis set. Adiabatic absorption energies, the difference between the minima of the ground and S_1 states, were computed for the naphthalene and anthracene monomers using each method for which excited-state gradients were available. Relaxation of monomer and dimer structures in the S_1 state performed using B3LYP TDDFT gradients has a minor impact on intramolecular and intermolecular C–C distances (≈ 0.02 Å), including a breaking of the six-fold symmetry of the benzene in the $(BN)^*$ complex (Tables S2-S5). Geometry changes are small enough, though, that we expect relative trends in exciplex binding energy to apply to both relaxed and unrelaxed structures.
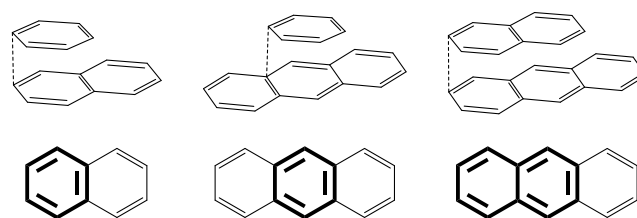

Figure 1: Eclipsed geometries from side and top perspectives for $(BN)^*$ (left), $(BA)^*$ (center), and $(NA)^*$ (right). The intermolecular coordinate r_z is marked with a dotted line.

The binding energy E_B is defined as

$$E_B = |E(r_z = r_0) - E(r_z = 10 \text{ Å})|, \quad (1)$$

where r_0 is the minimum-energy intermolecular separation. It is important to note that the lowest-energy singlet excited state for the separated monomers ($r_z = 10$ Å) has the larger monomer in the first excited state (S_1) and the smaller monomer in the ground state (S_0) because the $S_0 \rightarrow S_1$ transition energy decreases with increasing acene size. This configuration serves as the reference in E_B calculations. Excimers have degenerate reference states. The excitation energies corresponding to vertical monomer absorption, ΔE_V, and adiabatic monomer absorption, ΔE_A, refer to the excitation energy of the larger monomer in the complex for the same reason.

3. Results and Discussion

Error in the TDDFT Description of Exciplex Binding

For (BN)*, the potential energies computed for varying r_z (Fig. 2) at the NEVPT2/cc-pVDZ level yield an E_B value of 18.16 kJ/mol (Table 1). The complex has an approximate complete basis set limit binding energy of 19.2 kJ/mol,[32] more than 30% higher than the CCSD(T)-corrected DFT binding energy for the ground state complex in an eclipsed configuration (≈ 14.5 kJ/mol).[69] This difference suggests that exciplex stabilization is an important contributor to the complex's S_1 binding energy. Error due to the use of the DMRG approach is estimated at ≈ 1 kJ/mol based on E_B convergence with M for this complex.[32]

The shape and well depth of the intermolecular exciplex potential energy surface varies significantly between the TDDFT calculations performed using different exchange-correlation functionals. The LC-BLYP functional has a binding energy 54% lower than the NEVPT2/cc-pVDZ result. The tuned LC-BLYP functionals perform better—the LC-BLYP-TM functional yields a binding energy 28% too low, while the LC-BLYP-TD functional comes within 7% of the correct result. For $r_z \geq 4.5$ Å, all of the LC-BLYP functionals are in excellent agreement, suggesting that

relative energy is insensitive to γ outside the region of the global minimum, and the choice to tune γ based on the global minimum geometry is justified.

While another range-separated functional, ωB97, matches the NEVPT2 potential energy surface extremely well around the minimum, it underbinds the complex in the 4-6 Å region, even slightly overshooting the $r_z = 10$ Å value around 5 Å. The ωB97X-D3 functional corrects this error, but shows an extremely shifted minimum. The r_0 of 3.69 Å would be more characteristic of a ground-state aromatic complex. The hybrid functionals both overbind the complex, but the BHandHLYP functional, with a significantly larger proportion of exact exchange, performs much better. The B3LYP functional E_B value is more than double the NEVPT2 one, while the B2PLYP functional overbinds the complex by 80%. The dispersion contribution to E_B provided by the D3 correction is significant. Without this correction, the B3LYP and BHandHLYP functionals do not show an attractive exciplex interaction (Fig. S2). The uncorrected B2PLYP functional still shows a stabilizing interaction, with the MP2 component of the double-hybrid functional likely capturing a portion of the dispersion energy. The ADC(2) method is significantly overbinding, yielding an E_B more than twice as high as the NEVPT2 result. The r_0 obtained is also more than 0.1 Å smaller than the next-smallest r_0.

The (BA)* exciplex, not surprisingly, is bound more strongly than (BN)*, with an NEVPT2 binding energy of 27.69 kJ/mol. Similar E_B trends are observed in results from the LC-BLYP and LC-BLYP-TM functionals (Fig. 3). For this complex, the LC-BLYP-TD improves on the LC-BLYP-TM result by only ≈ 1.5 kJ/mol.

E_B values for the ωB97X-D3 functional are now too high, and both the ωB97 and ωB97X-D3 functionals display an apparent instability in the 3.1-3.2 Å region, resulting in linear regions in the potential energy curves to the left of r_0. Hybrid and double hybrid results match the NEVPT2 curve closely, with B2PLYP and B3LYP results almost identical

and slightly overbinding.

Similar behavior is observed for the hybrids and double hybrid in the $(NA)^*$ system (Fig. 4), although a few differences from the other exciplexes are noticeable. In the absence of the D3 correction, the three hybrid and double hybrid functionals still show a stabilizing exciplex interaction (Fig. S2). Among the range-separated functionals, the LC-BLYP-TM and LC-BLYP-TD binding energies are larger than the ωB97 and ωB97X-D3 ones. The ωB97 functional shows unusual behavior around r_0, while the ωB97X-D3 functional r_0 is again dramatically shifted toward high r_z values, a geometry error accompanied by a binding energy more than 50% too low. As in the case of $(BN)^*$, tuning the LC-BLYP functional for the complex rather than the larger monomer alone improves the binding energy—by approximately 10 kJ/mol for this complex. This LC-BLYP-TD E_B value falls within 1 kJ/mol of the NEVPT2 reference, though the r_0 obtained is more than 0.15 Å too low, consistent with most of the other functionals.

Table 1: Binding Energies E_B and Optimal S_1 Intermolecular Separations r_0 for $(BN)^*$, $(BA)^*$, and $(NA)^*$

	$(BN)^*$		$(BA)^*$		$(NA)^*$	
Excitation Type	L_b		L_a		L_a	
Method	E_B (kJ/mol)	r_0 (Å)	E_B (kJ/mol)	r_0 (Å)	E_B (kJ/mol)	r_0 (Å)
NEVPT2	18.16	3.34	27.69	3.28	49.30	3.34
ADC(2)	38.60	3.00	46.58	3.16	92.10	3.05
LC-BLYP	8.37	3.41	10.78	3.49	25.04	3.25
LC-BLYP-TM	13.06	3.25	15.93	3.40	40.26	3.21
LC-BLYP-TD	16.97	3.17	17.47	3.35	48.90	3.19
ωB97	17.13	3.48	21.39	3.44	37.28	3.40
ωB97X-D3	15.46	3.69	29.34	3.47	27.04	3.71
BHandHLYP	24.79	3.25	25.94	3.42	53.63	3.25
B2PLYP	32.67	3.15	34.40	3.33	73.97	3.19
B3LYP	42.08	3.13	32.69	3.33	76.90	3.23

Separating the exciplexes into those derived from L_a states of the larger monomer and those derived from L_b states (Fig. 5) is a useful first step in analyzing trends in TDDFT error. ΔE_V and ΔE_A values suggest that, between the anthracene and naphthalene parent monomers, the L_b naphthalene excitation represents a greater challenge than the L_a anthracene excitation. Every ΔE_V value computed for naphthalene (Table 2) overshoots the estimated experimental value by at least 30 kJ/mol. The trend among ΔE_A values is similar. The difference between ΔE_V and ΔE_A results is related to the quality of the exited-state potential energy surface, and the differences obtained for naphthalene are noticeably smaller than the estimated experimental difference. The NEVPT2 ΔE_V reported here is approximately 27 kJ/mol higher than the ΔE_V value reported for a similar CASPT2 calculation.[73] Based on additional NEVPT2 calculations, we attribute ≈ 6 kJ/mol of this difference to the difference in monomer geometries used (B3LYP/def2-TZVP in this work vs. MP2/6-31G*), and a further ≈ 6 kJ/mol to the different NEVPT2 basis sets (cc-pVDZ in this work vs. TZVP). The additional 15 kJ/mol difference may be attributed to the different perturbative correction approach (NEVPT2 vs CASPT2). For anthracene, though, values of ΔE_A and ΔE_V are generally in better agreement with experiment, and the agreement between computed and experimental $\Delta E_V - \Delta E_A$ values is excellent.

When E_B values for the exciplexes are considered, though, the pattern becomes more complex. To provide more examples of each type, the L_a- and L_b-derived states of $(NN)^*$ in the eclipsed configuration are also considered. It is immediately apparent that the B2PLYP and B3LYP functionals perform much better for L_a-derived states than for L_b-derived states, with no meaningful difference between the two functionals for L_a-derived states. Both functionals predict L_b vertical excitation energies for the naphthalene monomer that are in excellent agreement with the NEVPT2 excitation energy (Table 2), so the error stems from problems with the description of the exciplex in its minimum-energy conformation.

The ωB97 and ωB97X-D3 functionals perform well for L_b-derived states, despite the fact that their ΔE_V values are 20-30 kJ/mol higher than the NEVPT2 ones. The fact that this destabilization of the excited monomer does not lead to overbinding indicates that the exciplex with $r_z = r_0$ is destabilized to a similar degree. For L_a-derived states more strongly bound than

Table 2: Monomer S_1 Absorption Energies ΔE_V and ΔE_A.

Method	Naphthalene (L_b)			Anthracene (L_a)		
	ΔE_V (kJ/mol)	ΔE_A (kJ/mol)	ΔE_V-ΔE_A (kJ/mol)	ΔE_V (kJ/mol)	ΔE_A (kJ/mol)	ΔE_V-ΔE_A (kJ/mol)
LC-BLYP	453.8	448.3	5.5	383.0	366.4	16.6
LC-BLYP-TM	444.6	437.2	7.4	365.0	347.6	17.4
ωB97	466.6	456.2	10.4	391.8	373.3	18.5
ωB97X-D3	457.1	448.9	8.2	378.1	360.6	17.5
BHandHLYP	463.2	458.7	4.5	363.2	347.2	16.0
B3LYP	433.3	422.8	10.5	330.6	313.5	17.1
NEVPT2	436.4	–	–	366.3	–	–
ADC(2)	440.9	–	–	368.5	–	–
B2PLYP	431.0	–	–	346.7	–	–
Exptl.	398.8[a]	383.1[b]	15.7	347.7[a]	331.0[c]	16.7

[a]Estimated vertical excitation energies with solvent correction[26] derived from experimental 0–0 excitation energies.[70] [b]Ref.[71] [c]Ref.[72]
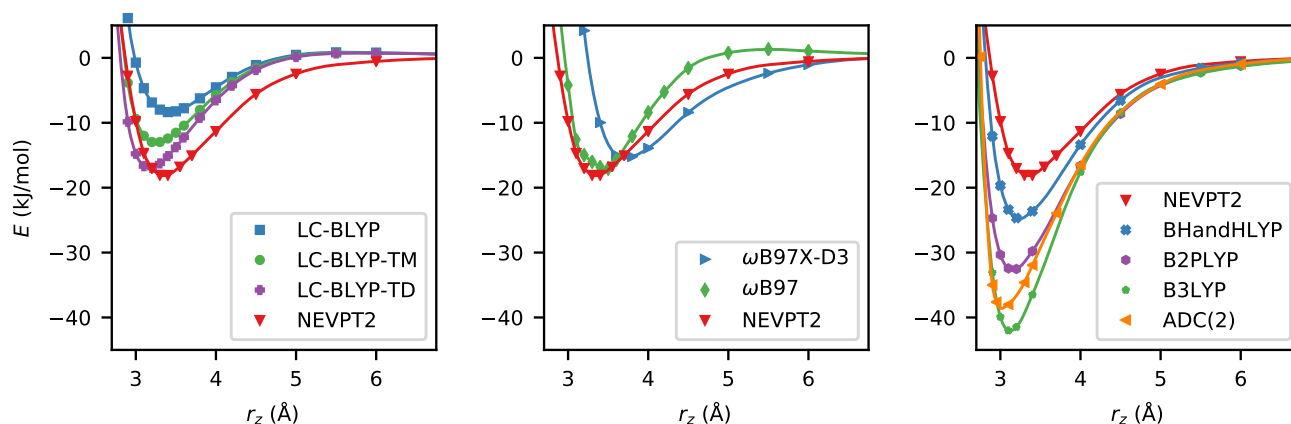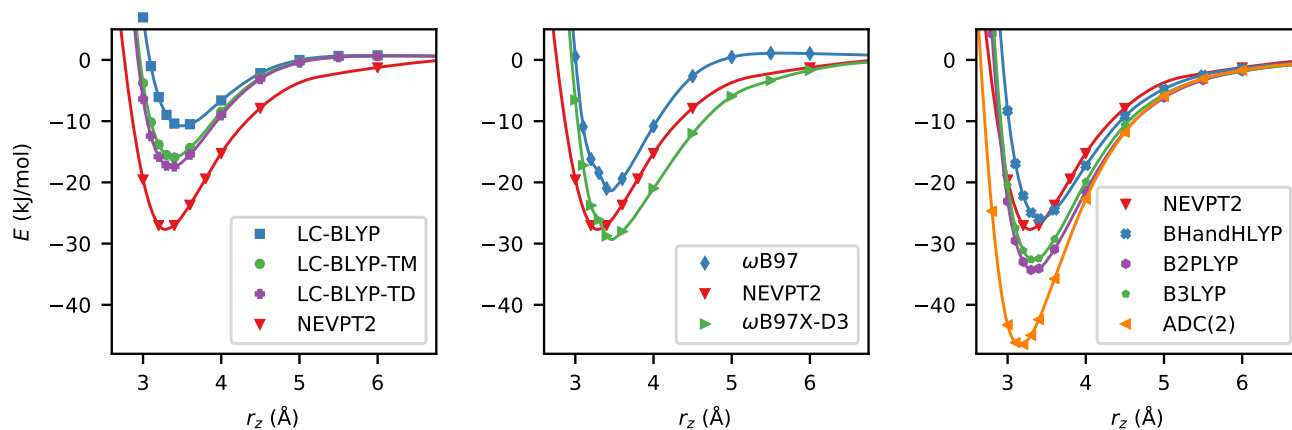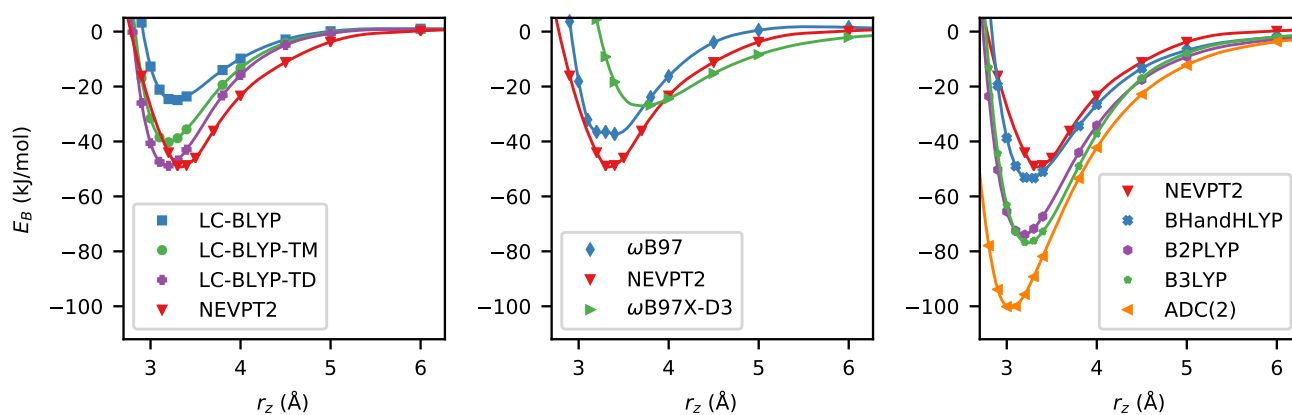

Figure 2: S_1 potential energies for (BN)* relative to $r_z = 10$ Å. Lines have been added to guide the eye.

(BA)*, both functionals are underbinding, although the ordering of the two E_B values varies between complexes.

A difference between E_B results for L_a- and L_b-derived states is also apparent for the BHandHLYP functional. For L_b-derived states, the functional is uniformly overbinding, a result consistent with a good description of the exciplex but a high L_b excitation energy for the naphthalene monomer. The L_a excitation energy for naphthalene is not correspondingly high, resulting in an L_b–L_a gap of only 8

kJ/mol, when experimental reports range from 45-70 kJ/mol.[30] This depressed L_a energy likely contributes to the most notable BHandHLYP E_B error, observed for the L_a-derived naphthalene excimer.

Perhaps the most consistent TDDFT errors are observed from the LC-BLYP and tuned LC-BLYP functionals. The tuned functionals in particular yield reasonable ΔE_V values, although absolute error does increase with increasing interaction strength. A similar L_a–L_b energy difference for the naphthalene monomer

Figure 3: S$_1$ potential energies for (BA)* relative to $r_z = 10$ Å.

Figure 4: S$_1$ potential energies for (NA)* relative to $r_z = 10$ Å.
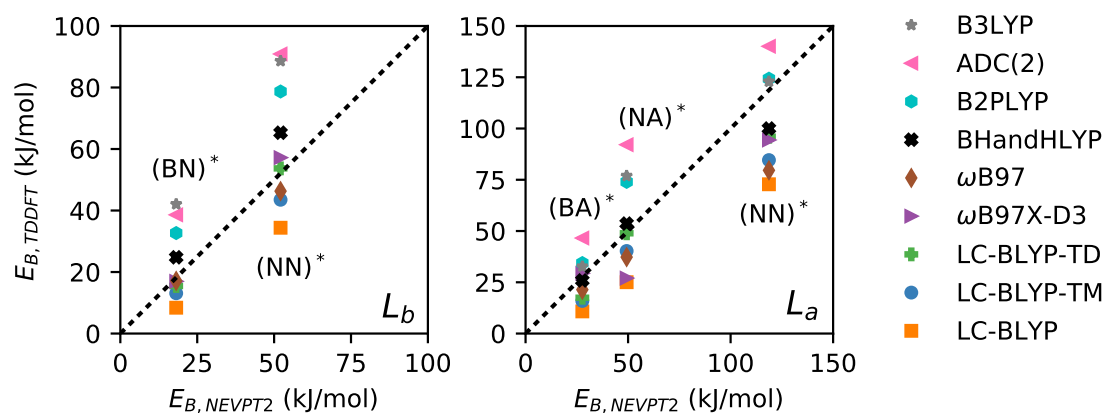
Figure 5: TDDFT binding energies E_B as a function of NEVPT2 binding energies for exciplexes in the L_b state (left) and the L_a state (right). For the naphthalene excimers, CASPT2/cc-pVDZ binding energies[30] are substituted for NEVPT2 values.
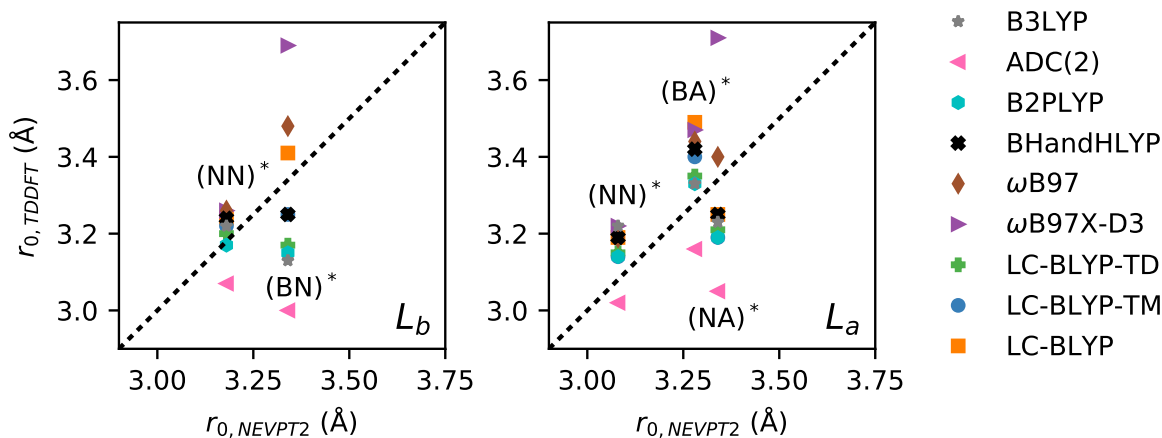
Figure 6: TDDFT optimal intermolecular separations r_0 as a function of NEVPT2 r_0 values for exciplexes in the L_b state (left) and the L_a state (right). For the naphthalene excimers, CASPT2/cc-pVDZ r_0 values[30] are substituted for NEVPT2 results.

of approximately 30 kJ/mol is obtained from all three LC-BLYP functionals. Although smaller than the reported NEVPT2 energy difference, this result is at least on the same order of magnitude. E_B errors of 20-40% are observed for all exciplexes, suggesting that the under-stabilization of minimum-energy exciplexes might have a uniform cause for both L_a- and L_b-derived states.

Errors in r_0, illustrated in Fig. 6, do not show a uniform dependence on the exciplex state. For the more tightly-bound exciplexes (NEVPT2 $r_0 < 3.25$ Å), all results agree within ≈ 0.1 Å. Error increases significantly for the more loosely-bound complexes. The B2PLYP and B3LYP functionals give r_0 values approximately 0.2 Å too small for the L_b-derived (BN)*, but perform very well for the L_a-derived (BA)*. The r_0 values obtained from the ωB97X-D3 functional vary unpredictably—for (NA)*, the r_0 obtained is 0.37 Å too high.

The most consistent errors overall in both E_B and r_0 values are observed for the ADC(2) method. ADC(2) ΔE_V results for both naphthalene and anthracene monomers are in excellent agreement with the NEVPT2 values. However, the complexes are uniformly overbound, with absolute E_B errors in the 20-40 kJ/mol range, and the r_0 values obtained are all 0.05-0.1 Å too low. This overbinding may
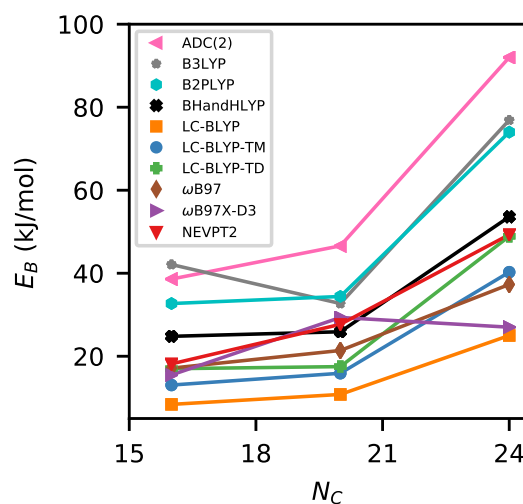

Figure 7: Binding energy E_B as a function of the number of carbons N_C in each exciplex.

be due in part to the commonly-observed tendency of the MP2 method—which supplies the ground state energy in ADC(2) calculations—to overbind van der Waals complexes. Using a larger basis set seems unlikely to alleviate the issue, as recalculation of the binding energy of (BN)* using the cc-pVTZ basis at the cc-pVDZ minimum geometry and reference configuration yields an even higher binding energy of 45.5 kJ/mol, and repeating the procedure for (BA)* results in $E_B = 46.89$, a value virtually identi-

cal to the cc-pVDZ result.

Beyond reproducing individual binding energies, it is desirable for functionals to capture the relationships between the E_B values obtained for each complex. The ωB97X-D3 and B3LYP functionals fail to capture the monotonic increase in E_B values with respect to complex mass (Fig. 7). The remaining functionals severely underestimate difference in E_B values for (BN)* and (BA)*. The NEVPT2 E_B results for the two differ by more than 50% (9.5 kJ/mol), while the maximum obtained is 29% (2.4 kJ/mol) from the LC-BLYP functional.

Physical Origins of Exciplex Stabilization

It remains, then, to rationalize both TDDFT errors and the observed NEVPT2 trends in exciplex binding energy. The binding energies of ground-state noncovalent aromatic complexes scale approximately linearly with the number of carbon atoms in the complex N_C.[14–16,74,75] This is not the case for the exciplexes considered here (Fig. 7). For (BN)* and (BA)*, the ratios of $E_{B,NEVPT2}$ to N_C are 1.16 kJ/mol and 1.15 kJ/mol, respectively. For (NA)*, the ratio is 2.05 kJ/mol.

Considering the form of the natural orbitals involved in the electronic transitions can help shed light on their varying character. Natural transition orbitals (NTOs) have been calculated for each exciplex using one generally overbinding functional, B2PLYP, and one underbinding functional, LC-BLYP-TM. For (BN)*, the difference between the E_B values obtained from each is high—the B2PLYP E_B is 80% too high, and the LC-BLYP-TM E_B is 28% too low. In both sets of NTOs (Fig. 8), the electron density is shifted toward the naphthalene monomer, suggesting that the exciplex excitation is principally a naphthalene excitation. However, this shift is more dramatic for the LC-BLYP-TM NTOs. The LC-BLYP-TM bonding orbitals show significantly less electron density in the intermolecular region. Differences in electron density between the ground and excited states (Fig. S3) show a similar contrast between the two functionals, with the B2PLYP functional

yielding a larger area of enriched electron density between the molecules.

To quantify the degree of exciton delocalization and the charge transfer contribution, statistical descriptors based on the one-electron transition density matrix formulated by Plasser and coworkers.[31,76] These descriptors have been calculated for the B2PLYP functional and the LC-BLYP-TM functional (Table 3). Charge transfer number CT ranges from zero for a completely localized Frenkel excitation to unity for complete charge transfer. For the L_a-derived state of the naphthalene excimer, CT = 0.5, indicating equal charge transfer and localized excitation character.[31]

The participation ratio PR of each monomer in the excitation represents a second measure of excitation delocalization, with PR = 2 in the case of a symmetric excimer like (NN)*, where the two indistinguishable monomers participate equally. The average exciton position, POS, ranges from 1-2, POS = 1, 2 corresponds to exciton localization on a single monomer, and maximally delocalized excited states have POS = 1.5. For the mixed exciplexes, POS = 1 indicates exciton localization on the smaller monomer and POS = 2 indicates localization on the larger monomer. Population analysis for the electron and hole created by the excitation has also been performed to locate the charge carriers on specific monomers.

For (BN)*, the picture that emerges from both functionals is one in which the excitation is primarily localized on the naphthalene monomer, but not exclusively—it is spatially shifted in the direction of the benzene monomer, which has nonzero electron and hole populations. However, the degree of delocalization varies noticeably between the two functionals, with the overbinding B2PLYP functional producing additional exciton delocalization. The difference in CT values is particularly apparent, with the B2PLYP CT almost 80% higher than the LC-BLYP-TM CT.

In the case of (BA)*, the exciton descriptors obtained using each functional are much more similar, and considering the NTOs for the exciplex (Fig. 9) suggests why this might be the case—the electron density is located almost en-
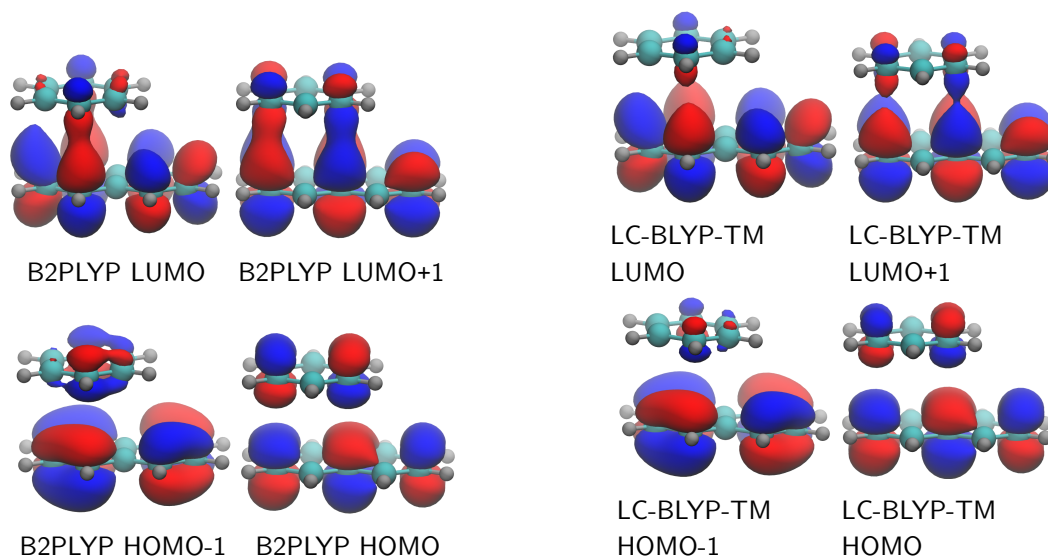
Figure 8: Frontier natural transition orbital isosurfaces for (BN)*.

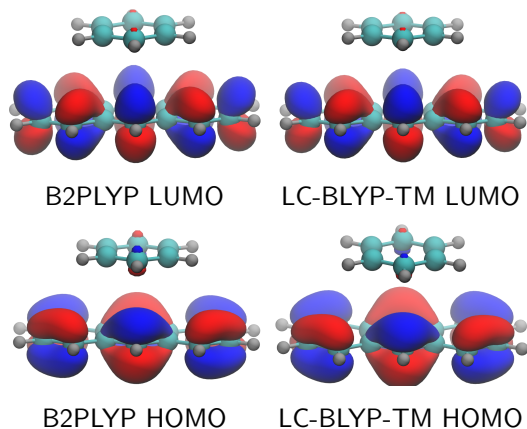Figure 9: Frontier natural transition orbital isosurfaces for (BA)*.
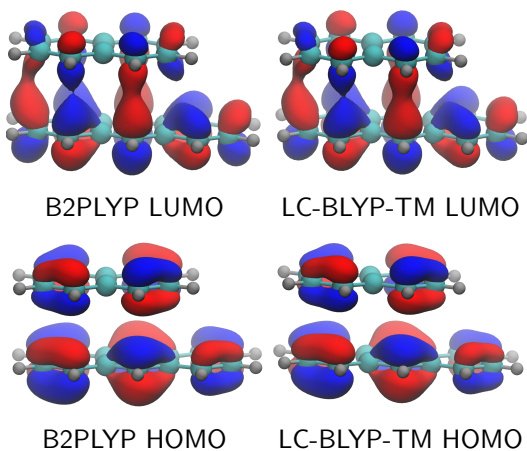

Figure 10: Frontier natural transition orbital isosurfaces for (NA)*.

tirely on the anthracene monomer, particularly for the bonding LUMO orbitals. With CT < 0.1 and PR < 1.1, it is clear that (BA)* would be better described as BA*.

If so, why is the per-carbon binding energy so similar to the one obtained for (BN)*, where moderate exciplex stabilization is present? The larger size of the BA compared to BN suggests enhanced noncovalent interactions regardless of electronic state, and electronic excitation can increase the polarizability of aromatics.[77] Thus, the excitation of the anthracene monomer may increase the interaction strength even without notable exciton delocalization. The fact that the excitation is largely localized on the anthracene monomer likely also explains why the performance of the LC-BLYP-TM and LC-BLYP-TD functionals was so similar for (BA)*; the electronic state of the benzene molecule remains nearly unchanged, so including it in the structure used for tuning does not significantly improve the description of the excited complex.

Although the NEVPT2 binding energy for (BA)* falls between the LC-BLYP-TM and B2PLYP ones, it is significantly larger than the calculated (BN)* NEVPT2 binding energy. Examination of the canonical HOMO orbitals obtained in the NEVPT2 calculation reveals a small amount of electron density on the benzene monomer (Fig. S4). Orbitals plotted with the same isovalue obtained from the LC-BLYP-TM

and B2PLYP calculations do not show this density, suggesting that both functionals may underestimate the $(BA)^*$ PR value—an error that would not be uncovered by considering each binding energy in isolation. Shorter intermolecular distances are generally associated with increased orbital overlap and thus increased possibility for exciton delocalization. Differences in the observed levels of exciton delocalization, then, are consistent with differences in r_0, which is overestimated by every DFT functional relative to the NEVPT2 result, regardless of the absolute binding energies obtained.

Finally, the binding energies obtained from the two functionals for $(NA)^*$ are in better agreement, each falling within 30% of the NEVPT2 result. The geometric agreement is striking; r_0 values differ by less than 0.02 Å, and the NTOs are virtually identical (Fig. 10). With CT $\approx$ 0.35 and PR $>$ 1.5, the charge transfer and exciton delocalization contributions to stabilization of $(NA)^*$ are the largest obtained for any of the exciplexes. The similarity of the exciton delocalization descriptors obtained using both functionals reflects the smaller relative error of each as well as the geometric similarity.

4. Conclusions

In this work, we have reported the binding energies, geometries, and exciton properties of three acene exciplexes. These represents the first theoretical investigation of the benzene-anthracene and naphthalene-anthracene exciplexes, and the first TDDFT investigation of the benzene-naphthalene exciplex. CASSCF/NEVPT2 benchmark calculations have been performed to account for multireference character. We have shown that the benzene-naphthalene and naphthalene-anthracene exciplexes are stabilized by a moderate degree of exciton delocalization over both monomers and charge transfer that is revealed by analysis of TDDFT one-electron transition density matrices. The exciton in the benzene-anthracene complex is shown to be localized almost entirely on the anthracene monomer, perhaps because the large

difference in the energies of each monomer's frontier orbitals inhibit their mixing and thus the formation of bonding orbitals. In every case, though, the degree of stabilization makes the electronic structure of the mixed exciplexes distinct from both the parent monomers and excimers of the parent monomers, an experimentally observable effect that should be accounted for in interpretation of fluorescence spectra.

The difficulties involved with calculating accurate valence excitation energies for acenes using TDDFT are well known, but this work also demonstrates that the accuracy of exciplex binding energies depends on the character of the monomer excited state from which the exciplex is derived. Binding energy errors are not easily predictable from the magnitude of the monomer excitation energy error. Double-hybrid functionals offer advantages over hybrid GGAs in providing a balanced description of both states, but strong overbinding is still observed for L_b-derived states. Significant variation is observed among the range-separated functionals considered, with functionals in the ωB97 family yielding inconsistent results. While the LC-BLYP functional is extremely underbinding for all complexes, tuning the range-separation parameter for each complex, or even for the larger monomer in each complex, improves binding energies significantly. The performance of each functional considered is summarized in Table S6. Despite many promising results, it is clear that noncovalent excited-state interactions remain a significant challenge for TDDFT methods.

Supporting information

Values of γ for tuned LC-BLYP functionals, bond lengths for structures optimized in the excited state, binding curves calculated without the D3 correction, difference densities for S_1 excitations, NEVPT2 orbitals for BA, qualitative functional quality table.

Table 3: Statistical descriptors for (BN)*, (BA)*, and (NA)* computed using the S_1 TDDFT one-electron transition density matrices at r_0.

Complex	Functional	CT	PR	POS	Large Monomer h+ pop.	e- pop.	Small Monomer h+ pop.	e- pop.
(BN)*	B2PLYP	0.254	1.415	1.821	0.778	0.824	0.197	0.151
	LC-BLYP-TM	0.142	1.272	1.879	0.846	0.874	0.133	0.105
(BA)*	B2PLYP	0.060	1.063	1.969	0.945	0.936	0.025	0.034
	LC-BLYP-TM	0.053	1.058	1.972	0.926	0.928	0.027	0.026
(NA)*	B2PLYP	0.354	1.560	1.765	0.712	0.768	0.255	0.199
	LC-BLYP-TM	0.349	1.546	1.771	0.713	0.766	0.246	0.193

References

(1) Scholes, G. D.; Ghiggino, K. P. Electronic Interactions and Interchromophore Excitation Transfer. *J. Phys. Chem.* **1994**, *98*, 4580–4590.

(2) East, A. L. L.; Lim, E. C. Naphthalene Dimer: Electronic States, Excimers, and Triplet Decay. *J. Chem. Phys.* **2000**, *113*, 8981–8994.

(3) Birks, J. B. *Photophysics of Aromatic Molecules*; Wiley – Interscience: New York, 1970.

(4) Xia, J.; Sanders, S. N.; Cheng, W.; Low, J. Z.; Liu, J.; Campos, L. M.; Sun, T. Singlet Fission : Progress and Prospects in Solar Cells. *Adv. Mater.* **2017**, *29*, 1601652.

(5) Feng, X.; Krylov, A. I. On Couplings and Excimers: Lessons from Studies of Singlet Fission in Covalently Linked Tetracene Dimers. *Phys. Chem. Chem. Phys.* **2016**, *18*, 7751–61.

(6) Casanova, D. Bright Fission: Singlet Fission into a Pair of Emitting States. *J. Chem. Theory Comput.* **2015**, *11*, 2642–2650.

(7) Bardeen, C. J. The Structure and Dynamics of Molecular Excitons. *Annu. Rev. Phys. Chem.* **2013**, *65*, 127–148.

(8) Takaya, T.; Su, C.; de La Harpe, K.; Crespo-Hernandez, C. E.; Kohler, B. UV Excitation of Single DNA and RNA Strands Produces High Yields of Exciplex States Between Two Stacked Bases. *Proc. Natl. Acad. Sci.* **2008**, *105*, 10285–10290.

(9) Miller, J. H. Aromatic Excimers : Evidence for Polynuclear Aromatic Hydrocarbon Condensation in Flames. *Proc. Combust. Inst.* **2005**, *30*, 1381–1388.

(10) Adkins, E. M.; Giaccai, J. A.; Miller, J. H. Computed Electronic Structure of Polynuclear Aromatic Hydrocarbon Agglomerates. *Proc. Combust. Inst.* **2017**, *36*, 957–964.

(11) Michelsen, H. A. Probing Soot Formation, Chemical and Physical Evolution, and Oxidation: A Review of in Situ Diagnostic Techniques and Needs. *Proc. Combust. Inst.* **2017**, *36*, 717–735.

(12) Wang, H. Formation of Nascent Soot and Other Condensed-Phase Materials in

Flames. *Proc. Combust. Inst.* **2011**, *33*, 41–67.

(13) Adamson, B. D.; Skeen, S. A.; Ahmed, M.; Hansen, N. Detection of Aliphatically Bridged Multi-Core Polycyclic Aromatic Hydrocarbons in Sooting Flames with Atmospheric-Sampling High-Resolution Tandem Mass Spectrometry. *J. Phys. Chem. A* **2018**, acs.jpca.8b08947.

(14) Podeszwa, R.; Szalewicz, K. Physical Origins of Interactions in Dimers of Polycyclic Aromatic Hydrocarbons. *Phys. Chem. Chem. Phys.* **2008**, *10*, 2735–2746.

(15) Ehrlich, S.; Moellmann, J.; Grimme, S. Dispersion-Corrected Density Functional Theory for Aromatic Interactions in Complex Systems. *Acc. Chem. Res.* **2013**, *46*, 916–926.

(16) Lee, N. K.; Park, S.; Kim, S. K. Ab Initio Studies on the van der Waals Complexes of Polycyclic Aromatic Hydrocarbons. I. Benzene-Naphthalene Complex. *J. Chem. Phys.* **2002**, *116*, 7910–7917.

(17) Lee, N. K.; Park, S.; Kim, S. K. Ab Initio Studies on the van der Waals Complexes of Polycyclic Aromatic Hydrocarbons. II. Naphthalene Dimer and Naphthalene-Anthracene Complex. *J. Chem. Phys.* **2002**, *116*, 7910–7917.

(18) Jara-Cortés, J.; Rocha-Rinza, T.; Hernández-Trujillo, J. Electron Density Analysis of Aromatic Complexes in Excited Electronic States: The Benzene and Naphthalene Excimers. *Comput. Theor. Chem.* **2015**, *1053*, 220–228.

(19) Rocha-Rinza, T.; Vico, L. D.; Veryazov, V.; Roos, O. A Theoretical Study of Singlet Low-Energy Excited States of the Benzene Dimer. *Chem. Phys. Lett.* **2006**, *426*, 268–272.

(20) Rocha-Rinza, T.; Christiansen, O. Linear Response Coupled Cluster Study of the Benzene Excimer. *Chem. Phys. Lett.* **2009**, *482*, 44–49.

(21) Diri, K.; Krylov, A. I. Electronic States of the Benzene Dimer: A Simple Case of Complexity. *J. Phys. Chem. A* **2012**, *116*, 653–662.

(22) van Duijneveldt, F. B.; van Duijneveldt-van de Rijdt, J. G. C. M.; van Lenthe, J. H. State of the Art in Counterpoise Theory. *Chem. Rev.* **1994**, *94*, 1873–1885.

(23) Miliordos, E.; Aprà, E.; Xantheas, S. S. Benchmark Theoretical Study of the π-π Binding Energy in the Benzene Dimer. *J. Phys. Chem. A* **2014**, *118*, 7568–7578.

(24) Orchin, M.; Jaffè, H. H. *Symmetry, Orbitals, and Spectra*; Wiley: New York, 1971.

(25) Prlj, A.; Sandoval-Salinas, M. E.; Casanova, D.; Jacquemin, D.; Corminboeuf, C. Low-Lying pi-pi* States of Heteroaromatic Molecules: A Challenge for Excited State Methods. *J. Chem. Theory Comput.* **2016**, *12*, 2652–2660.

(26) Grimme, S.; Parac, M. Substantial Errors from Time-Dependent Density Functional Theory for the Calculation of Excited States of Large π Systems. *Chemphyschem* **2003**, *4*, 292–295.

(27) Kuritz, N.; Stein, T.; Baer, R.; Kronik, L. Charge-Transfer-Like $\pi\pi^*$ Excitations in Time-Dependent Density Functional Theory: A Conundrum and its Solution. *J. Chem. Theory Comput.* **2011**, *7*, 2408–2415.

(28) Richard, R. M.; Herbert, J. M. Time-Dependent Density-Functional Description of the 1La State in Polycyclic Aromatic Hydrocarbons: Charge-Transfer Character in Disguise? *J. Chem. Theory Comput.* **2011**, *7*, 1296–1306.

(29) Goerigk, L.; Grimme, S. Double-Hybrid Density Functionals Provide a Balanced Description of Excited ^1L_a and ^1L_b States in Polycyclic Aromatic Hydrocarbons. *J.*

Chem. Theory Comput. **2011**, *7*, 3272–3277.

(30) Shirai, S.; Kurashige, Y.; Yanai, T. Computational Evidence of Inversion of ^1L_a and ^1L_b-Derived Excited States in Naphthalene Excimer Formation from ab Initio Multireference Theory with Large Active Space: DMRG-CASPT2 Study. *J. Chem. Theory Comput.* **2016**, *12*, 2366–2372.

(31) Plasser, F.; Lischka, H. Analysis of Excitonic and Charge Transfer Interactions from Quantum Chemical Calculations. *J. Chem. Theory Comput.* **2012**, *8*, 2777–2789.

(32) Krueger, R. A.; Blanquart, G. Multireference Exciplex Binding Energies: Basis Set Convergence and Error. *Int. J. Quantum Chem.* **2019**, *119*, e25819.

(33) Trofimov, A. B.; Schirmer, J. An Efficient Polarization Propagator Approach to Valence Electron Excitation Spectra. *J. Phys. B: At. Mol. Opt. Phys.* **1995**, *28*, 2299–2324.

(34) Angeli, C.; Cimiraglia, R.; Evangelisti, S.; Leininger, T.; Malrieu, J. P. Introduction of n-Electron Valence States for Multireference Perturbation Theory. *J. Chem. Phys.* **2001**, *114*, 10252.

(35) Schapiro, I.; Sivalingam, K.; Neese, F. Assessment of n-Electron Valence State Perturbation Theory for Vertical Excitation Energies. *J. Chem. Theory Comput.* **2013**, *9*, 3567–3580.

(36) Dunning, T. H. Gaussian Basis Sets for Use in Correlated Molecular Calculations. I. The Atoms Boron Through Neon and Hydrogen. *J. Chem. Phys.* **1989**, *90*, 1007–1023.

(37) Chan, G. K.-L.; Keselman, A.; Nakatani, N.; Li, Z.; White, S. R. Matrix Product Operators, Matrix Product States, and Ab Initio Density Matrix Renormalization Group Algorithms. *J. Chem. Phys.* **2016**, *014102*, 014102.

(38) Chan, G. K.-L.; Dorando, J. J.; Ghosh, D.; Hachmann, J.; Neuscamman, E.; Wang, H.; Yanai, T. In *Frontiers in Quantum Systems in Chemistry and Physics*; Wilson, S., Grout, P. J., Maruani, J., Delgado-Barrio, G., Piecuch, P., Eds.; Springer Netherlands: Dordrecht, 2008; pp 49–65.

(39) Chan, G. K. L.; Head-Gordon, M. Highly Correlated Calculations with a Polynomial Cost Algorithm: A Study of the Density Matrix Renormalization Group. *J. Chem. Phys.* **2002**, *116*, 4462–4476.

(40) Guo, S.; Watson, M. A.; Hu, W.; Sun, Q.; Chan, G. K. L. N-Electron Valence State Perturbation Theory Based on a Density Matrix Renormalization Group Reference Function, with Applications to the Chromium Dimer and a Trimer Model of Poly(p-Phenylenevinylene). *J. Chem. Theory Comput.* **2016**, *12*, 1583–1591.

(41) Olivares-Amaya, R.; Hu, W.; Nakatani, N.; Sharma, S.; Yang, J.; Chan, G. K.-L. The Ab-Initio Density Matrix Renormalization Group in Practice. *J. Chem. Phys.* **2015**, *142*, 34102.

(42) Sun, Q.; Berkelbach, T. C.; Blunt, N. S.; Booth, G. H.; Guo, S.; Li, Z.; Liu, J.; McClain, J.; Sayfutyarova, E. R.; Sharma, S. et al. The Python-based Simulations of Chemistry Framework (PySCF). *Wiley Interdiscip. Rev. Comput. Mol. Sci.* **2017**, *e1340*.

(43) Sharma, S.; Chan, G. K.-L. Spin-Adapted Density Matrix Renormalization Group Algorithms for Quantum Chemistry. *J. Chem. Phys.* **2012**, *136*, 124121.

(44) Sayfutyarova, E. R.; Sun, Q.; Chan, G. K. L.; Knizia, G. Automated Construction of Molecular Active Spaces from Atomic Valence Orbitals. *J. Chem. Theory Comput.* **2017**, *13*, 4063–4078.

(45) Stephens, P. J.; Devlin, F. J.; Chabalowski, C. F.; Frisch, M. J. Ab Initio

Calculation of Vibrational Absorption and Circular Dichroism Spectra Using Density Functional Force Fields. *J. Phys. Chem.* **1994**, *98*, 11623–11627.

(46) Becke, A. D. A New Mixing of Hartree-Fock and Local Density-Functional Theories. *J. Chem. Phys.* **1993**, *98*, 1372–1377.

(47) Grimme, S. Semiempirical Hybrid Density Functional with Perturbative Second-Order Correlation. *J. Chem. Phys.* **2006**, *124*, 034108.

(48) Head-Gordon, M.; Rico, R. J.; Oumi, M.; Lee, T. J. A Doubles Correction to Electronic Excited States from Configuration Interaction in the Space of Single Substitutions. *Chem. Phys. Lett.* **1994**, *219*, 21–29.

(49) Grimme, S.; Ehrlich, S.; Goerigk, L. Effect of the Damping Function in Dispersion Corrected Density Functional Theory. *J. Comput. Chem.* **2010**, *31*, 2967–2970.

(50) Huenerbein, R.; Grimme, S. Time-Dependent Density Functional Study of Excimers and Exciplexes of Organic Molecules. *Chem. Phys.* **2008**, *343*, 362–371.

(51) Briggs, E. A.; Besley, N. A. Modelling Excited States of Weakly Bound Complexes with Density Functional Theory. *Phys. Chem. Chem. Phys.* **2014**, *16*, 14455–14462.

(52) Weigend, F.; Hser, M.; Patzelt, H.; Ahlrichs, R. RI-MP2: Optimized Auxiliary Basis Sets and Demonstration of Efficiency. *Chem. Phys. Lett.* **1998**, *294*, 143–152.

(53) Chai, J. D.; Head-Gordon, M. Systematic Optimization of Long-Range Corrected Hybrid Density Functionals. *J. Chem. Phys.* **2008**, *128*, 084106.

(54) Lin, Y.-S.; Li, G.-D.; Mao, S.-P.; Chai, J.-D. Long-Range Corrected Hybrid Density Functionals with Improved Dispersion Corrections. *J. Chem. Theory Comput.* **2013**, *9*, 263–272.

(55) Stein, T.; Kronik, L.; Baer, R. Reliable Prediction of Charge Transfer Excitations in Molecular Complexes Using Time-Dependent Density Functional Theory. *J. Am. Chem. Soc.* **2009**, *131*, 2818–2820.

(56) Leininger, T.; Stoll, H.; Werner, H.-J.; Savin, A. Combining Long-Range Configuration Interaction with Short-Range Density Functionals. *Chem. Phys. Lett.* **1997**, *275*, 151–160.

(57) Weigend, F.; Ahlrichs, R. Balanced Basis Sets of Split Valence, Triple Zeta Valence and Quadruple Zeta Valence Quality for H to RN: Design and Assessment of Accuracy. *Phys. Chem. Chem. Phys.* **2005**, *7*, 3297–3305.

(58) Weigend, F. Hartree-Fock Exchange Fitting Basis Sets for H to RN. *J. Comput. Chem.* **2008**, *29*, 167–175.

(59) Laurent, A. D.; Blondel, A.; Jacquemin, D. Choosing an Atomic Basis Set for TD-DFT, SOPPA, ADC(2), CIS(D), CC2 and EOM-CCSD Calculations of Low-Lying Excited States of Organic Dyes. *Theor. Chem. Acc.* **2015**, *134*, 1–11.

(60) Sure, R.; Brandenburg, J. G.; Grimme, S. Small Atomic Orbital Basis Set First-Principles Quantum Chemical Methods for Large Molecular and Periodic Systems: A Critical Analysis of Error Sources. *ChemistryOpen* **2016**, *5*, 94–109.

(61) Dreuw, A.; Wormit, M. The Algebraic Diagrammatic Construction Scheme for the Polarization Propagator for the Calculation of Excited States. *Wiley Interdiscip. Rev. Comput. Mol. Sci.* **2015**, *5*, 82–95.

(62) Neese, F. The ORCA Program System. *Wiley Inderdiscip. Rev. Comput. Mol. Sci.* **2012**, *2*, 73–78.

(63) Plasser, F. TheoDORE 1.0: A Package for Theoretical Density, Orbital Relaxation, and Exciton Analysis. http://theodore-qc.sourceforge.net.

(64) Humphrey, W.; Dalke, A.; Schulten, K. VMD – Visual Molecular Dynamics. *J. Molec. Graphics* **1996**, *14*, 33–38.

(65) Iyer, E. S. S.; Sadybekov, A.; Lioubashevski, O.; Krylov, A. I.; Ruhman, S. Rewriting the Story of Excimer Formation in Liquid Benzene. *J. Phys. Chem. A* **2017**, *121*, 1962–1975.

(66) Dubinets, N. O.; Safonov, A. A.; Bagaturyants, A. A. Structures and Binding Energies of the Naphthalene Dimer in Its Ground and Excited States. *J. Phys. Chem. A* **2016**, *120*, 2779–2782.

(67) Casanova, D. Theoretical Investigations of the Perylene Electronic Structure: Monomer, Dimers, and Excimers. *Int. J. Quantum Chem.* **2015**, *115*, 442–452.

(68) Amicangelo, J. C. Theoretical Study of the Benzene Excimer Using Time-Dependent Density Functional Theory. *J. Phys. Chem. A* **2005**, *109*, 9174–9182.

(69) Bludský, O.; Rubeš, M.; Soldán, P.; Nachtigall, P. Investigation of the Benzene-Dimer Potential Energy Surface: DFT/CCSD(T) Correction Scheme. *J. Chem. Phys.* **2008**, *128*.

(70) Biermann, D.; Schmidt, W. Diels-Alder Reactivity of Polycyclic Aromatic Hydrocarbons. 1. Acenes and Benzologs. *J. Am. Chem. Soc.* **1980**, *102*, 3163–3173.

(71) Reylè, C.; Brèchignac, P. Fluorescence of Jet-Cooled Naphthalene: Emission Spectra, Lifetimes and Quantum Yields. *Eur. Phys. J. D* **2000**, *8*, 205–210.

(72) Staicu, A.; Rouillè, G.; Sukhorukov, O.; Henning, T.; Huisken, F. Cavity Ring-Down Laser Absorption Spectroscopy of Jet-Cooled Anthracene. *Mol. Phys.* **2004**, *102*, 1777–1783.

(73) Schreiber, M.; Silva-Junior, M. R.; Sauer, S. P.; Thiel, W. Benchmarks for Electronically Excited States: CASPT2, CC2, CCSD, and CC3. *J. Chem. Phys.* **2008**, *128*.

(74) Wang, W.; Sun, T.; Zhang, Y.; Wang, Y. B. The Benzene - - - Naphthalene Complex: A More Challenging System than the Benzene Dimer for Newly Developed Computational Methods. *J. Chem. Phys.* **2015**, *143*, 0–6.

(75) Fedorov, I. A.; Zhuravlev, Y. N.; Berveno, V. P. Structural and Electronic Properties of Perylene from First Principles Calculations. *J. Chem. Phys.* **2013**, *138*, 1–6.

(76) Plasser, F.; Bäppler, S. A.; Wormit, M.; Dreuw, A. New Tools for the Systematic Analysis and Visualization of Electronic Excitations. II. Applications. *J. Chem. Phys.* **2014**, *141*, 024107.

(77) Benchea, A. C.; Babusca, D.; Morosanu, A. C.; Dimitriu, D. G.; Dorohoi, D. O. Excited State Molecular Polarizability Estimated by Solvatochromic Means. *AIP Conf. Proc.* **2017**, *1796*, 030013.

TOC image